The Astronomical Journal, 133:1287–1301, 2007 April

NEAR-INFRARED PROPERTIES OF 24 GLOBULAR CLUSTERS IN THE GALACTIC BULGE[1]

E. Valenti
European Southern Observatory, Santiago, Chile; and INAF–Osservatorio Astronomico di Bologna, Bologna, Italy; evalenti@eso.org

F. R. Ferraro
Bologna University, Bologna, Italy

and

L. Origlia
INAF–Osservatorio Astronomico di Bologna, Bologna, Italy
Received 2006 July 28; accepted 2006 November 28

ABSTRACT

We present near-IR color-magnitude diagrams and physical parameters for a sample of 24 Galactic globular clusters toward the bulge. In this paper we discuss the properties of 12 new clusters (out of the 24) in addition to those previously studied and published by our group. The compilation includes measurements of the cluster reddening, distance, photometric metallicity, horizontal branch red clump, and red giant branch morphological (e.g., mean ridgelines) and evolutionary (e.g., bump and tip) features. The compilation is available in electronic form on the World Wide Web, and it will be updated regularly.

Key words: Galaxy: bulge — globular clusters: general — infrared: stars — techniques: photometric

1. INTRODUCTION

In the last decades Galactic globular clusters (GCs) have proven to be extremely important astrophysical laboratories for a wide range of problematic issues. Indeed, the study of their stellar populations addresses fundamental questions ranging from stellar structure, evolution, and dynamics to Galaxy formation and the early epoch of the universe. Containing some of the oldest stars known, they are *fossils* from the remote and violent epoch of the formation of the Galaxy. They also serve as test particles for studying Galaxy dynamics and testing stellar dynamical models. Being the largest aggregates in which all post-main-sequence (post-MS) stars can be individually observed, they serve as fiducial templates for understanding the integrated light from distant, unresolved stellar systems. In this respect, the bulge GCs provide ideal templates for exploring the high-metallicity regime, and thus for studying the stellar content of extragalactic bulges and ellipticals. However, the high and patchy extinction, which makes optical observations difficult to impossible along most bulge lines of sight, coupled with the limited performances of the past generation of near-IR instrumentation, has prevented accurate determinations of the bulge GCs' basic properties (such as age, metallicity, and distance), which have already been known for a long time in the case of the halo clusters. The current generation of ground-based IR instrumentation, with high spatial resolution and wide field coverage, and the future availability of the *James Webb Space Telescope* will allow us to resolve the brightest giants in galaxies up to several megaparsecs away. Hence, a homogeneous compilation of the bulge GCs' properties to be used as empirical templates of metal-rich stellar populations is strongly urgent. In view of this, our group started a long-term project devoted to fully characterizing the stellar populations in the bulge GC system using color-magnitude diagrams (CMDs) and luminosity functions (LFs) in the near-IR (see Ferraro et al. 2000, hereafter F00; Valenti et al. 2004a, hereafter VFO04a; Valenti et al. 2004b, hereafter VFO04b; Valenti et al. 2004c; Valenti et al. 2005, hereafter VOF05; Origlia et al. 2005b, hereafter O05). The collected photometric database has been used to perform a detailed description of the main morphological and evolutionary features of the red giant branch (RGB) sequence, by means of a set of photometric indices that were defined and widely described in F00 and calibrated as a function of the cluster metallicity in VFO04a and VFO04b.

In this paper we present the largest homogeneous near-IR photometric database of bulge GCs ever obtained. For each cluster the compilation includes (1) the photometric catalog, (2) the RGB mean ridgeline, (3) accurate reddening, distance, and metallicity determinations, (4) the luminosity of the main RGB evolutionary features (e.g., the bump and the tip), and (5) the mean magnitude of the horizontal-branch red clump (HB-RC). Moreover, in order to be easily accessible by the community, the compilation will also be provided in electronic form.

The program cluster sample is presented in § 2, while § 3 is devoted to a detailed description of the observations, data reduction, and derived CMDs of a sample of 12 bulge clusters, recently observed and presented here for the first time. Section 4 describes the overall characteristics of the compilation and the measurement of the HB-RC and the RGB bump and tip.

2. THE ENTIRE SAMPLE

The cluster sample presented in this study contains 24 GCs in the bulge direction observed in the near-IR by our group in the last few years. The target selection was performed by defining "bulge GCs" as all those located within $|b| \leq 10^{\circ}$ and $|l| \leq 20^{\circ}$, where l and b are the Galactic coordinates, and giving the highest priority to the metal-rich population. Note that this definition is mainly a working hypothesis and refers only to the positions of the clusters in the bulge direction. However, there is growing evidence, based on kinematics (Dinescu et al. 2003) and high-resolution chemical abundances (Origlia et al. 2005a and references therein), favoring a bulge origin for the metal-rich GCs within 3 kpc of the Galactic center. Figure 1 shows the spatial distribution in Galactic coordinates of our sample (which counts 50%

[1] Based on data taken at the ESO New Technology Telescope, within the observing programs 73.D-0313, 75.D-0372, and 77.D-0757.

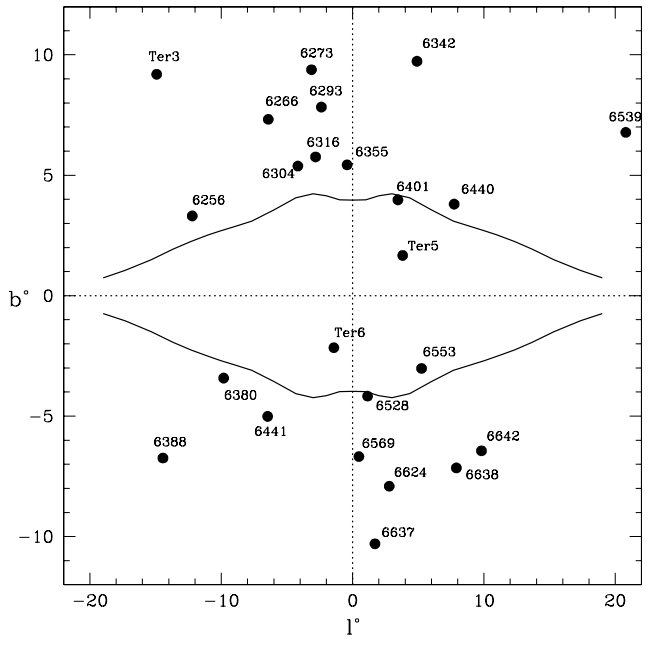

FIG. 1.—Position of the bulge cluster global sample with respect to the *COBE* DIRBE 3.5 μm inner bulge outline (*solid line*; Weiland et al. 1994) at 5 MJy sr^{-1}.

of the entire bulge GC system) and the *COBE* DIRBE 3.5 μm inner bulge outline (Weiland et al. 1994). The clusters discussed in this paper fall into three categories:

Sample A.—Seven clusters (NGC 6342, NGC 6380, NGC 6440, NGC 6441, NGC 6528, NGC 6553, and NGC 6624) have already been published, and a detailed description of the observations, data reduction, and analysis can be found in F00, VFO04a, and VFO04b. This sample has been used to perform a detailed analysis of the main RGB morphological and evolutionary features, leading to an empirical calibration of suitable near-IR photometric indices (e.g., RGB color, magnitude, slope, bump, and tip) as a function of the cluster metallicity.

Sample B.—Five clusters (NGC 6304, NGC 6569, NGC 6637, NGC 6638, and NGC 6539) were presented in VOF05 and O05, in which a detailed description of the derived IR CMDs and an analysis of the RGB properties can be found. For this sample we derived the clusters' metallicities using the calibration of VFO04a and VFO04b.

Sample C.—Twelve clusters (NGC 6256, NGC 6266, NGC 6273, NGC 6293, NGC 6316, NGC 6255, NGC 6388, NGC 6401, NGC 6642, Ter 3, Ter 5, and Ter 6) are presented and discussed here for the first time.

3. PROPERTIES OF SAMPLE C

For this sample, a detailed description of the observations, data reduction, CMDs, and physical properties of each cluster is provided in the following subsections.

3.1. *Observations and Data Reduction*

J, H, and K_s images of the clusters in sample C were obtained during three observing runs in 2004 June, 2005 July, and 2006 June using the near-IR camera SofI, mounted on the ESO New Technology Telescope. During the observing runs two sets of data were secured:

1. *Standard-resolution set*.—A series of images in the J, H, and K_s bands were obtained using SofI in large-field mode, characterized by a pixel size of 0.288″ and a total field of view of $4.9' \times 4.9'$. On average, the images are a combination of 42, 72, and 99 exposures, each one 3 s long, in the J, H, and K_s passbands, respectively.

2. *High-resolution set*.—High-resolution images of the inner region of each cluster were also secured using the SofI focal elongator, yielding a pixel size of 0.146″ and a total field of view of $2.49' \times 2.49'$. High-resolution images are an average of 30 single exposures 1.2 s long. All the secured images are roughly centered on the cluster center.

Note that the region covered by our observations allows us to sample a significant fraction of the total cluster light (typically ~80%–95%) in all the program clusters. During the eight nights of observations the average seeing was always quite good (FWHM ≈ 0.8–1). Every image has been background-subtracted using sky fields located several arcminutes away from the cluster center and flat-field-corrected using halogen lamp exposures, acquired with the standard SofI calibration setup.

Standard crowded-field photometry, including point-spread function modeling, was carried out on each frame using DAOPHOT II ALLSTAR (Stetson 1987). For each cluster, two photometric catalogs (derived from high- and standard-resolution images) listing the instrumental J, H, and K_s magnitudes were obtained by cross-correlating the single-band catalogs. The standard- and high-resolution catalogs were combined by means of a proper weighted average, weighting the high-resolution measurements in the innermost region of the cluster higher. In principle, this strategy allows us to minimize blending effects. The internal photometric accuracy was estimated from the rms frame-to-frame scatter of multiple star measurements. Over most of the RGB extension, the internal errors are quite low ($\sigma_J \sim \sigma_H \sim \sigma_K <$ 0.03 mag), increasing up to ~0.06 mag at $K_s \geq 16$.

The instrumental magnitudes were then converted into the Two Micron All Sky Survey (2MASS) photometric system,[2] and the star positions astrometrized onto 2MASS[3] as was done for the clusters in samples A and B.

Since for Terzan 6 only high-resolution data were acquired, we also used J, H, and K' images obtained with the IRAC2 camera (mounted on the ESO Max-Planck-Institut 2.2 m telescope) in order to cover a larger area ($\approx 4' \times 4'$). The derived calibrated catalog was then merged with that obtained from the SofI observations. Note that, as already discussed in Valenti et al. (2004c), the calibration of the K' IRAC2 photometry onto the K_s SofI photometry requires a negligible color term.

Figure 2 presents the derived IR CMDs of the global sample of 24 GCs. As shown in the figure, the photometric catalogs span the entire RGB extension, from the tip to ≈2–5 mag below the HB (depending on the cluster extinction).

3.2. *Reddening, Distance, and Metallicity*

The main cluster properties such as reddening and distance were derived using a differential method based on the comparison of CMDs and LFs of clusters with similar HB morphology. However, this method allows one to derive reliable estimates of reddening and distance only for intermediate- to high-metallicity clusters, whose CMDs show a red clumpy HB morphology. In fact, the location in magnitude of the HB LF peak can be used as a reference feature and safely compared with that of the template cluster. In five metal-poor clusters (NGC 6256, NGC 6273, NGC 6293, NGC 6355, and NGC 6401) the blue HB morphology coupled with the relatively high reddening and the remarkable

[2] An overall uncertainty of ±0.05 mag in the zero-point calibration in all three bands has been estimated.

[3] The astrometric procedure provided rms residuals of ≈0.2″ in both right ascension and declination.

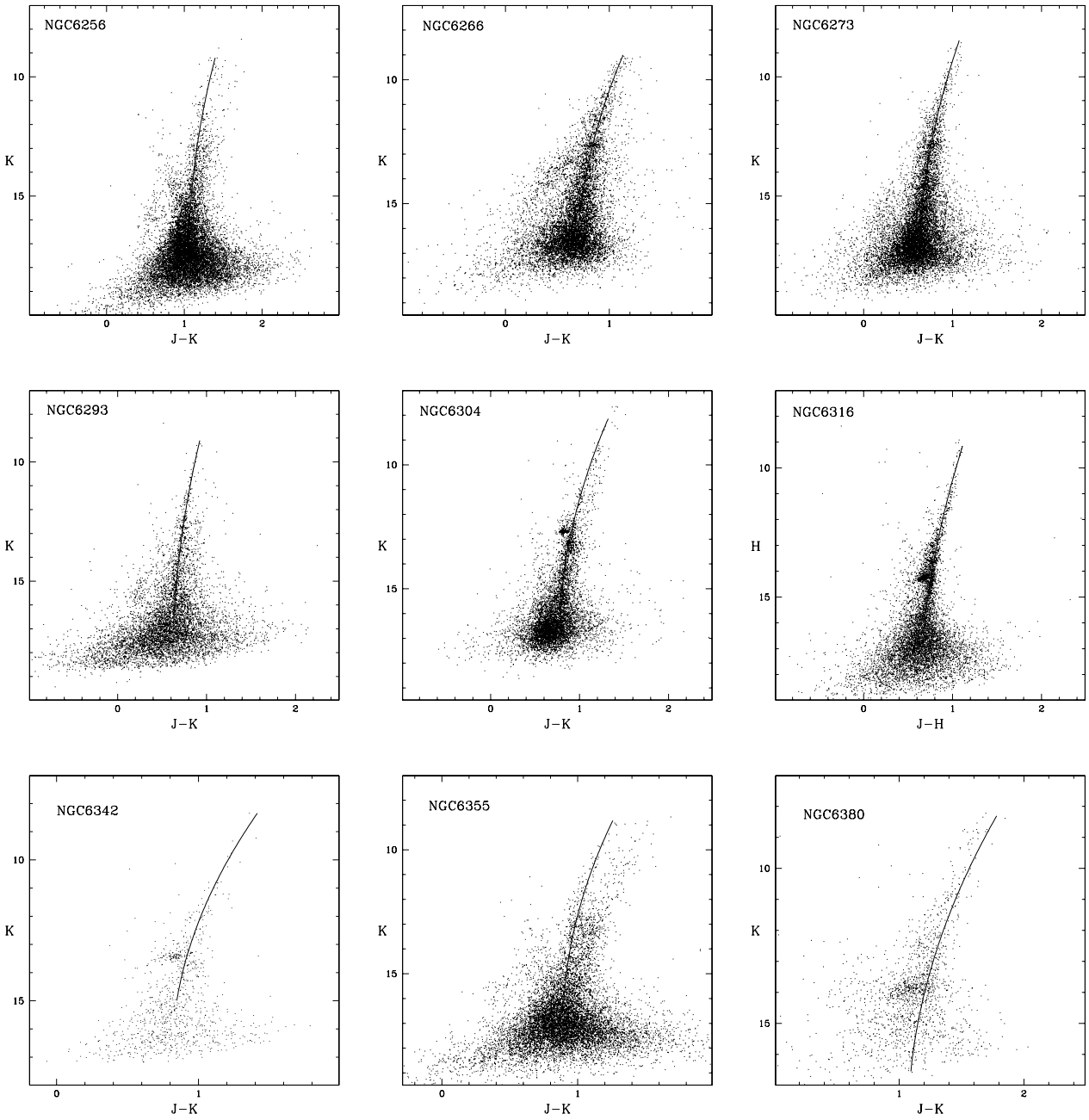

FIG. 2.—Observed near-IR CMDs and derived RGB ridgelines for the global cluster sample.

level of field contamination prevented a reliable determination of the HB level, and thus the use of the differential method. Hence, in these cases the cluster reddening and distance were obtained using the empirical method presented by Ferraro et al. (2006, hereafter FVO06), which allows one to simultaneously get the reddening, distance, and metallicity of a stellar system using a few observables, such as the RGB slope, tip, and mean ridgeline of the $[K, J-K]$ CMD.

The derived cluster reddening and distance were used to transform the observed CMDs and RGB ridgelines into the absolute plane, and to measure the following parameters: (1) the $(J-K)_0$ and $(J-H)_0$ colors at four fixed absolute magnitude levels ($M_K = M_H = -5.5, -5, -4$, and -3); (2) the absolute M_K and M_H magnitudes at constant $(J-K)_0 = (J-H)_0 = 0.7$ colors; and (3) the slope in the $[K, J-K]$- and $[H, J-H]$-planes. Then, using the empirical calibrations from VFO04a linking this set of photometric indices to the cluster metal content, we finally derived the photometric metallicity estimates in the Carretta & Gratton (1997) scale. Hence, hereafter the notation [Fe/H] refers to the Carretta & Gratton (1997) scale. Note that to derive the global metallicity [M/H], which takes into account the iron as well as the α-element abundances, we used the calibrations presented in FVO06 within the bulgelike enrichment scenario. Hence, according to Carney's (1996) suggestions and the more recent results on the bulge populations (Origlia et al. [2002, 2005a], Origlia & Rich [2004], Zoccali et al. [2004], O05, and Carretta et al. [2007] for bulge clusters, and Rich & Origlia [2005], Cunha & Smith [2006], Zoccali et al. [2006], and Fulbright et al. [2006] for giant field stars), we adopted $[\alpha/\mathrm{Fe}] = 0.30$ constant over the entire range of metallicity up to solar [Fe/H].

In the next subsections we present the CMDs and RGB fiducial ridgelines for the 12 bulge clusters of sample C. We briefly discuss

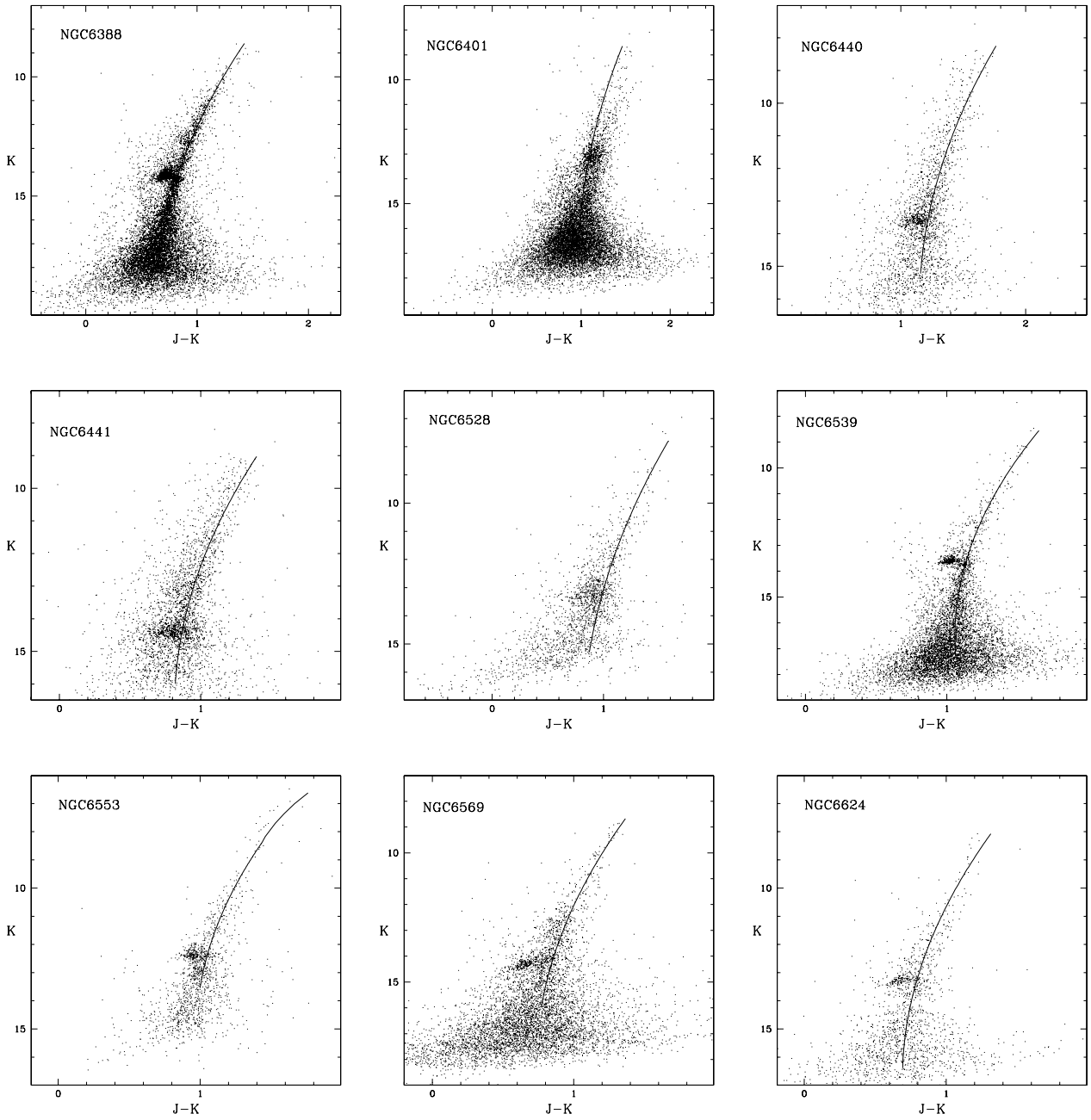

FIG. 2—*Continued*

the main CMD properties, and we provide some references for previously published photometries.

3.2.1. *NGC 6256*

NGC 6256 is a heavily reddened cluster in the outer bulge region. Its extinction, with estimates ranging from $E(B-V) = 0.84$ (Harris 1996, hereafter H96) to $E(B-V) = 1.66$ (Schlegel et al. 1998, hereafter S98), has prevented detailed photometric studies in the optical. Only two studies of the cluster can be found in the literature: the first by Barbuy et al. (1998a) based on *VI* ground-based photometry, and the second by Piotto et al. (2002) based on *Hubble Space Telescope* (*HST*) *BV* observations. However, the derived CMDs show an extremely scattered RGB that is barely defined.

In our IR CMD, shown in Figure 2, the cluster RGB is rather scattered, suggesting the presence of a red component that might be due to contamination by bulge field stars. The HB appears as a blue vertical structure at $(J-K) \sim 0.5$ and $K \leq 14$, typical of low to intermediate metallicity. The almost blue vertical sequence, at $11.5 \leq K \leq 15$ and $0.4 \leq (J-K) \leq 1$, is likely due to foreground disk stars. In order to investigate the nature of the observed RGB spread, we compared the sequence morphology in the CMDs at different distances from the cluster center (see Fig. 3). As shown in Figure 3, the reddest RGB component becomes progressively populated as the distance to the cluster center increases, thus confirming that it is due to field stars. As previously done for other highly contaminated clusters (see, e.g., NGC 6304 in VOF05), the RGB fiducial ridgeline was derived considering only the innermost region of the cluster, typically only the stars lying within $30''$ of the cluster center. Since the absence of a prominent feature such as the red clumpy HB makes it difficult to derive the cluster reddening and distance, we used the empirical

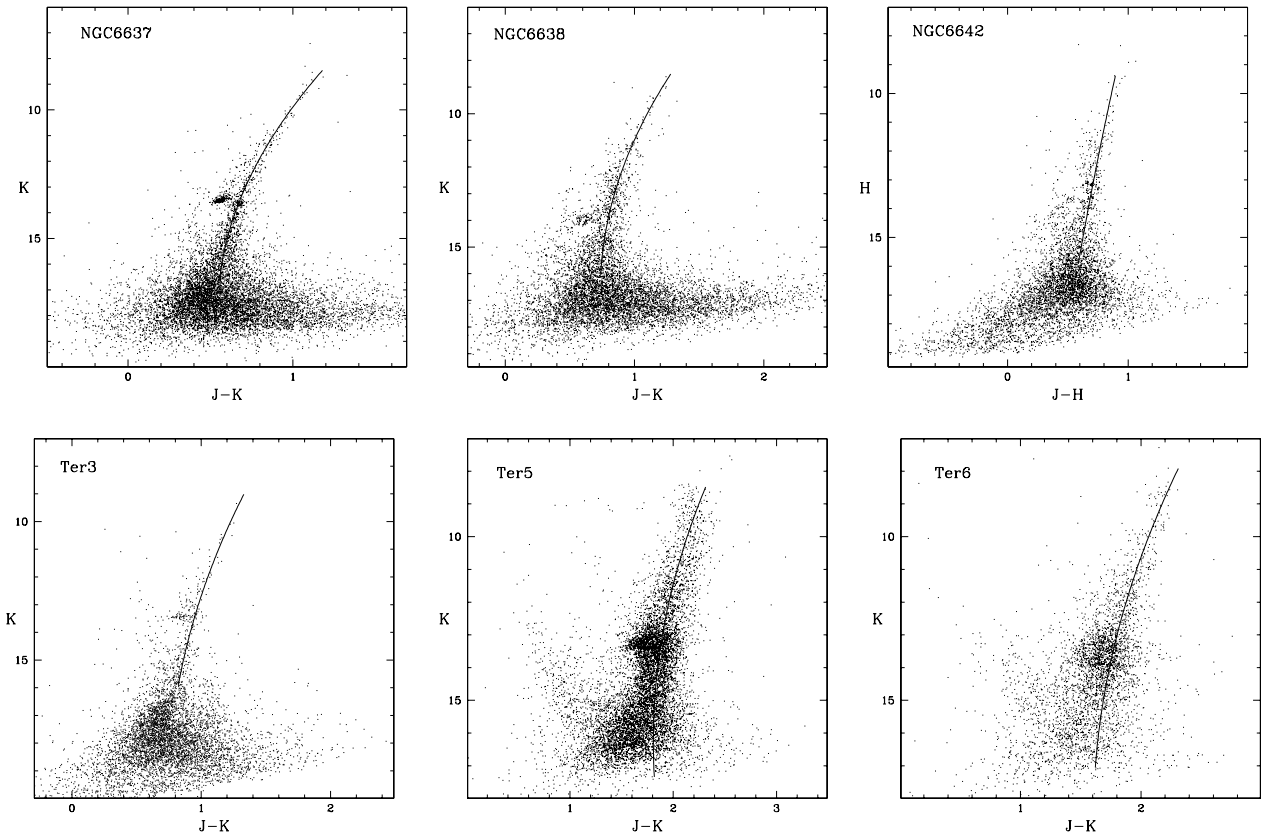

FIG. 2—*Continued*

method (see FVO06) rather than the differential one. From the analysis of the cluster CMD we estimated the RGB slope and the observed RGB tip to be $\mathrm{RGB}_{\mathrm{slope}} = -0.052$ and $K^{\mathrm{tip}} = 9.21$, respectively. Using these values as input parameters, the computational routine (assuming the bulgelike scenario) gives a reddening $E(B-V) = 1.2$, an intrinsic distance modulus $(m-M)_0 = 14.79$, and metallicities $[\mathrm{Fe/H}] = -1.63$ dex and $[\mathrm{M/H}] = -1.43$ dex. The distance estimate agrees with the value by H96, and the derived metallicity is consistent with those published by Stephens & Frogel (2004) ($[\mathrm{Fe/H}] = -1.35$ dex), based on low- to medium-resolution K spectra, and by Bica et al. (1998) ($[\mathrm{Fe/H}] = -1.01$ dex) from integrated optical spectroscopy.

3.2.2. *NGC 6266*

NGC 6266 is a high-density ($\log \rho \sim 5.34$; Djorgovski 1993), moderately reddened [$E(B-V) = 0.44$, H96; $E(B-V) = 0.47$, S98], massive ($M_V = -9.19$; H96) cluster that has been the subject of several dynamics, kinematics, and stellar variability studies. In fact, this cluster turns out to be particularly interesting because (1) it is the fifth-ranking (after Ter 5, 47 Tuc, M15, and M28) GC for wealth of millisecond pulsars (MSPs), and it is the only GC exclusively populated by MSPs in binary systems (Possenti et al. 2003); (2) it hosts more than 200 RR Lyrae variables (Contreras et al. 2005), whose periods place this cluster in the Oosterhoff type I group, although the cluster HB morphology (a blue HB component and a very extended blue tail) is similar to Oosterhoff type II GCs; (3) recent *Chandra* X-ray observations have revealed a very large number of X-ray sources, suggesting the presence of a high number of cataclysmic (and/or interacting) binaries; and (4) its radial velocity is smaller than the escape velocity from the bulge, indicating that, whatever its origin, it will never escape from the bulge (Dinescu et al. 2003). Beccari et al. (2006) published the most extensive photometry based on a combination of multiband high-resolution *HST* and wide-field ground-based observations aimed at studying the cluster dynamical state, finding that the cluster has not experienced core collapse yet. No IR photometric studies for this cluster have been published so far.

The observed CMD in the $[K, J-K]$-plane (see Fig. 2) shows a well-populated RGB and a blue extended HB, suggesting a low to intermediate metallicity. As expected, in the near-IR plane the high level of contamination by foreground disk stars affecting the optical ground-based CMD of Beccari et al. (2006) is drastically reduced, allowing us a clear definition of the RGB ridgeline from the tip down to the subgiant branch (SGB), at $K \sim 16$. To estimate the cluster metallicity, we have adopted the distance modulus $(m-M)_0 = 14.11$ of Beccari et al. (2006) (based on the Ferraro et al. [1999, hereafter F99] distance scale) and the reddening value from H96. The global set of photometric indices (in both the $[K, J-K]$- and $[H, J-H]$-planes) computed for NGC 6266 have yielded $[\mathrm{Fe/H}] = -0.98$ dex and $[\mathrm{M/H}] = -0.82$ dex, in good agreement with the values in the literature (see, e.g., H96).

3.2.3. *NGC 6273*

NGC 6273 is an intermediate- to low-metallicity ($[\mathrm{Fe/H}] = -1.68$; see H96), medium-concentration ($c = 1.5$; Djorgovski 1993) cluster, and it is also the second most luminous ($M_V = -9.50$) in the Djorgovski (1993) compilation. It has been the subject of a monographic study by Piotto et al. (1999) based on *HST BV* observations, aimed at understanding the nature of its extended HB blue tail, which shows a clear double-peaked distribution and a well-defined gap. From the analysis of the CMD the authors estimated an intrinsic distance modulus $(m-M)_0 = 14.77$

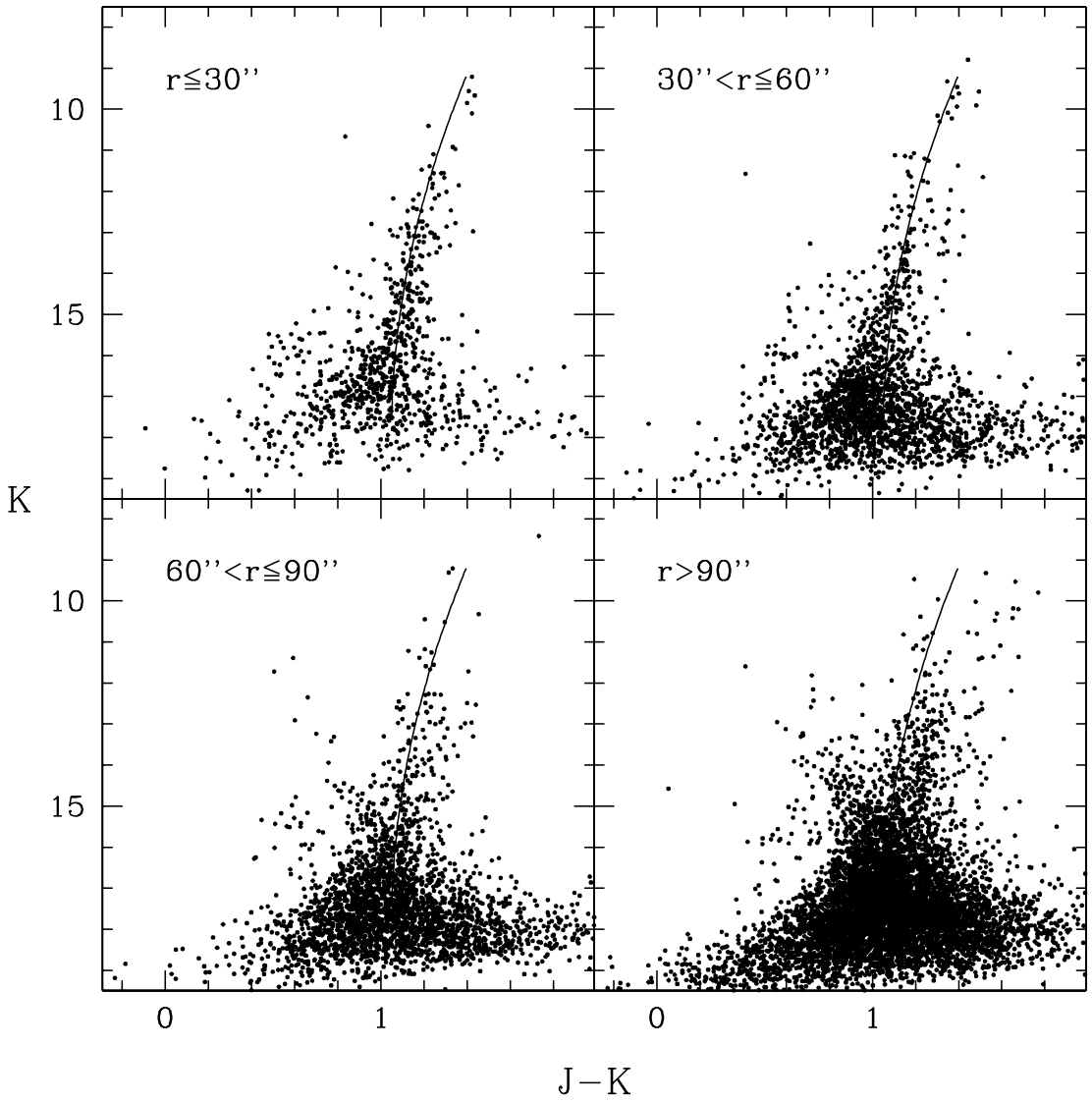

FIG. 3.—[$K, J-K$] CMDs of NGC 6256 at different distances (r) from the cluster center.

and an average reddening $E(B-V)=0.47$, although their optical CMD is strongly affected by differential reddening [$\Delta E(B-V)=0.2$ mag]. The only IR CMD available in the literature is the one published by Davidge (2000), but it is poorly populated and quite shallow, reaching only $K\sim 15$. From the [$K, J-K$] CMD, Davidge (2000) estimated a reddening $E(B-V)=0.38$, in excellent agreement with the value listed in the literature [i.e., $E(B-V)=0.38$, H96; $E(B-V)=0.31$, S98].

Figure 2 shows our observed CMD in the [$K, J-K$]-plane along with the derived RGB ridgeline (*solid line*). The cluster RGB is well populated even in the brightest magnitude bin, and the HB appears as a vertical structure almost parallel to the RGB at $(J-K)\sim 0.2$, suggesting a low to intermediate metallicity. Our photometry is deep enough to reach $\sim$1 mag below the main-sequence turnoff (MSTO); however, the SGB is quite scattered, preventing an accurate measurement of the MSTO luminosity, and hence a reliable cluster age estimate. Because of its HB morphology, the cluster reddening and distance were derived using the empirical method of FVO06. From the analysis of the observed CMD we derived the RGB slope ($\mathrm{RGB}_{\mathrm{slope}}=-0.063$) and the RGB tip ($K^{\mathrm{tip}}=8.57$). Adopting these two values as input parameters, we found $E(B-V)=0.40$, $(m-M)_0=14.58$, [Fe/H] $=-1.40$, and [M/H] $=-1.21$ for the cluster reddening, distance, and metallicity, respectively. The derived distance is consistent (within 0.2 mag) with the Piotto et al. (1999) estimate and (within 0.1 mag) with the value listed by H96. Our reddening measurement agrees well with the values in literature (see, e.g., H96; S98; Piotto et al. 1999; Davidge 2000).

3.2.4. *NGC 6293*

NGC 6293 is the most metal-poor cluster in the observed sample. In the literature, the best available photometries are those published by Davidge (2000) and Piotto et al. (2002). Piotto et al. (2002) presented an *HST* ($B, B-V$) CMD that shows an extended blue HB, confirming the low metal content of this cluster. The near-IR CMD of Davidge (2000) is poorly populated, and only reaches $K\sim 15$. From the IR data, the author estimated a reddening $E(B-V)=0.04$, which is significantly lower than the value listed in the literature [$E(B-V)=0.39$, H96; $E(B-V)=0.60$, S98]. A careful examination of the derived CMD in Figure 2 reveals the presence of a quite-scattered RGB, which cannot be explained in terms of photometric errors. In order to understand the nature of the observed scatter, as already done for NGC 6256, in Figure 4 we compared the radial CMDs in

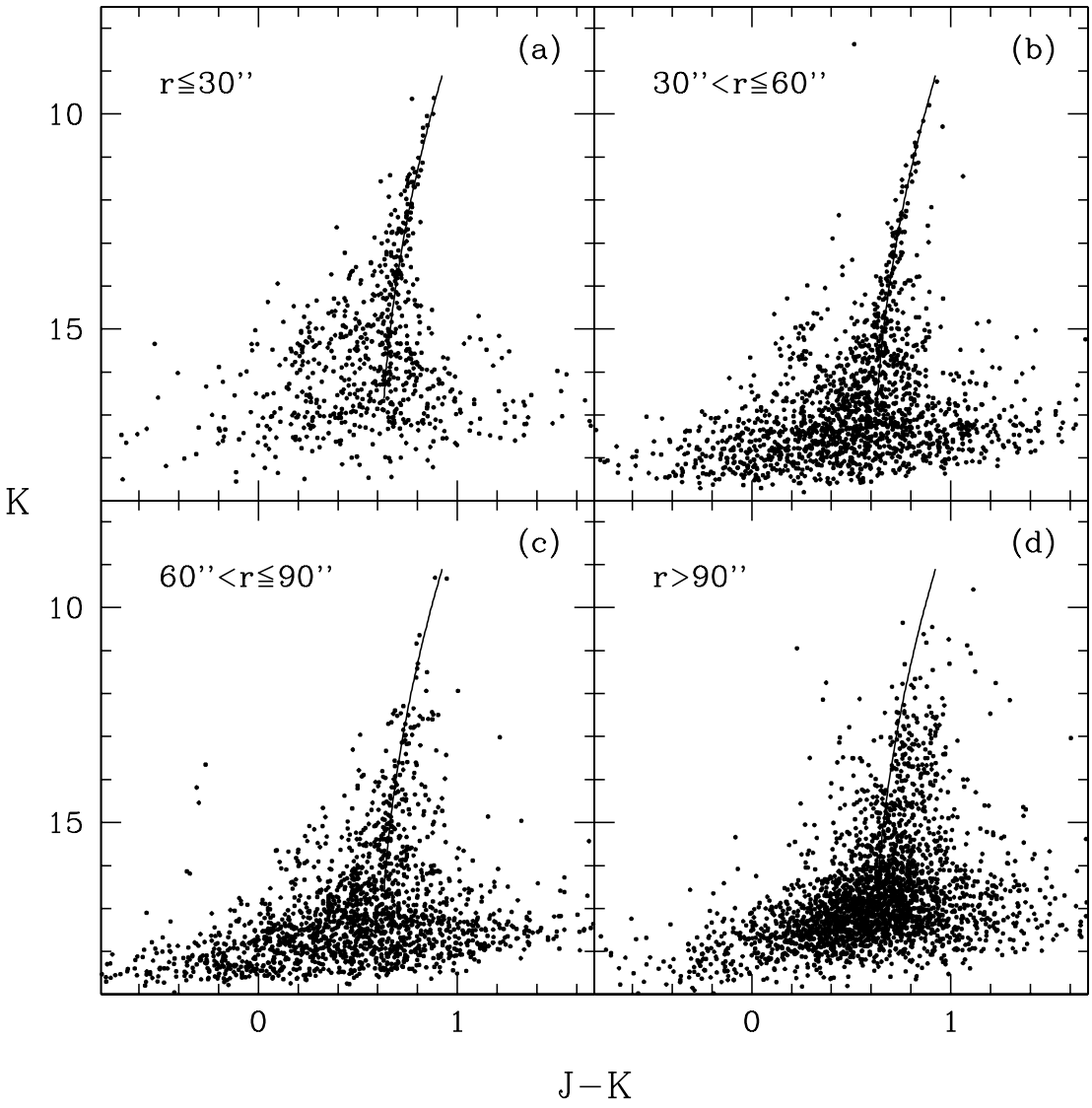

FIG. 4.—[$K, J - K$] CMDs of NGC 6293 at different distances (r) from the cluster center.

four annuli at different distances from the cluster center. In the innermost 30″ region (Fig. 4*a*) the RGB is quite narrow, and progressively spreads out with increasing distance from the cluster center. A field component redder than the cluster RGB is present at $r > 60''$. This high level of field contamination is not surprising, since NGC 6293 lies in the Ophiuchus complex, a dense stellar region toward the Galactic center. Hence, the RGB fiducial ridgeline was derived using only the stars in the innermost 30″ cluster region, where the field contamination is low. The measured reddening, distance, and metallicity estimates ($E(B - V) = 0.30$, $(m - M)_0 = 15.10$, $[\mathrm{Fe/H}] = -1.73$, and $[\mathrm{M/H}] = -1.55$) were obtained using the empirical method of FVO06, with the following input parameters: $\mathrm{RGB}_{\mathrm{slope}} = -0.048$ and $K^{\mathrm{tip}} = 9.24$. The derived cluster parameters nicely agree with the corresponding values listed by H96. In particular, the derived photometric metallicity is consistent (within ≈0.2 dex) with the spectroscopic estimate published by Lee & Carney (2002) (i.e., $[\mathrm{Fe/H}] = -1.99$ dex).

3.2.5. *NGC 6316*

Among the observed clusters, NGC 6316 is one of the most metal-rich and has the largest distance to the Galactic center. The [$K, V - K$] CMD presented by Davidge et al. (1992) shows a red clumpy HB and a quite well populated upper RGB, the photometry reaching only ∼1 mag below the HB. They estimated a reddening $E(B - V) = 0.6$, which is consistent within the values listed by H96 [$E(B - V) = 0.55$] and by S98 [$E(B - V) = 0.98$]. Piotto et al. (2002) presented a *HST* [$V, B - V$] CMD of this cluster, showing a HB morphology close to that of 47 Tuc. However, the moderately high reddening and the contamination by foreground disk stars prevented a clear definition of the RGB, which appears considerably scattered even in the brightest bins. As shown in Figure 2, our CMD in the [$H, J - H$]-plane is deep enough to properly sample the entire RGB, from the base up to the tip, thus allowing us a safe definition of the RGB fiducial ridgeline. From the CMD and the derived LF we estimated a reddening $E(B - V) = 0.56$, which is intermediate between the Davidge et al. (1992) and H96 estimates, and an intrinsic distance modulus $(m - M)_0 = 15.33$, slightly longer (∼0.13 mag) than the H96 value. Since no K-band data were taken for this cluster, to estimate its metallicity we only measured the photometric indices in the [$H, J - H$]-plane. Our findings, $[\mathrm{Fe/H}] = -0.60$ dex and $[\mathrm{M/H}] = -0.45$ dex, nicely agree with the value listed by H96, confirming that NGC 6316 has a metallicity slightly

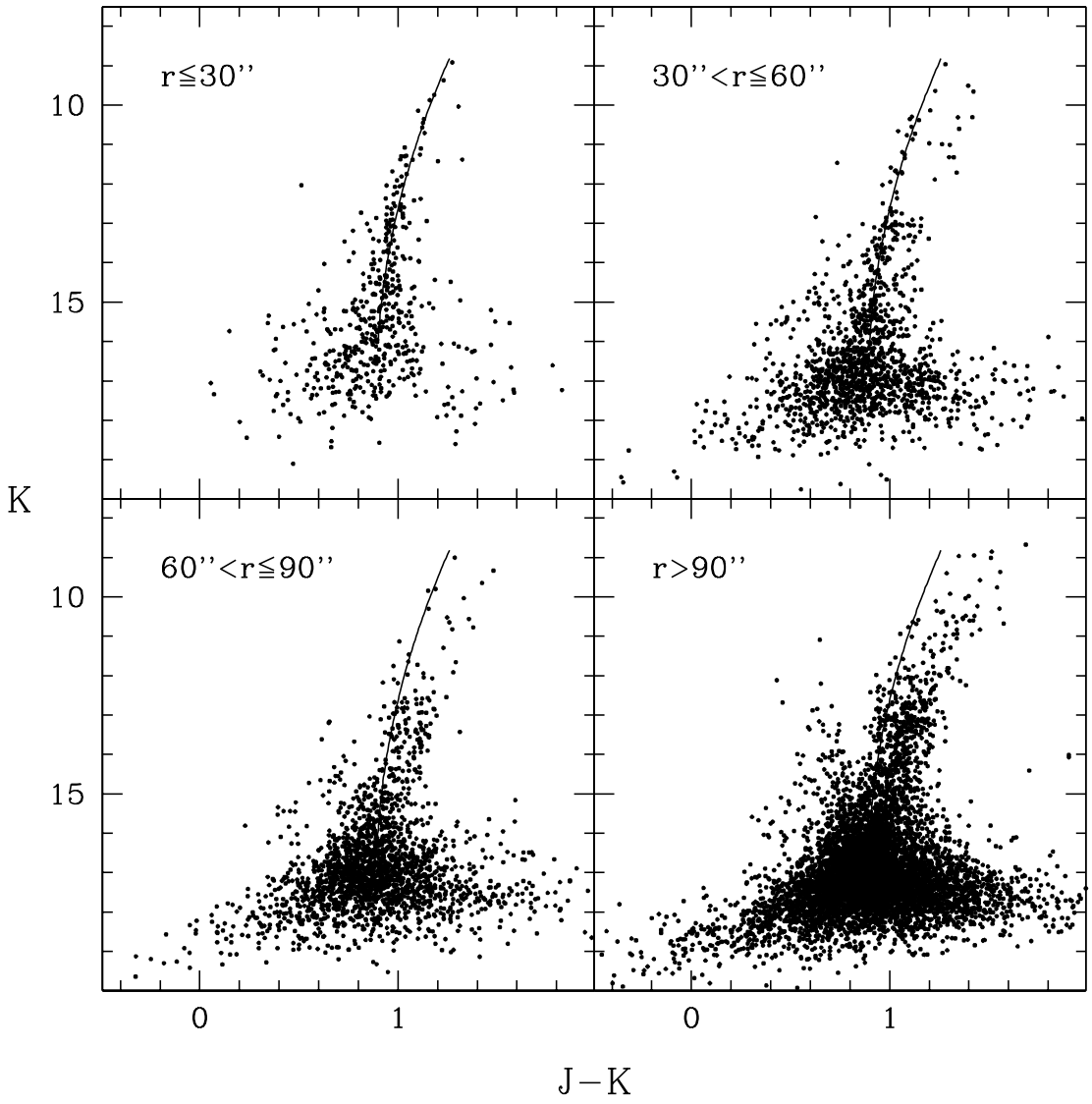

FIG. 5.—[$K, J-K$] CMDs of NGC 6355 at different distances (r) from the cluster center.

higher than 47 Tuc, as previously suggested by Davidge et al. (1992) on the basis of the RGB slope measurement.

3.2.6. *NGC 6355*

NGC 6355 lies behind a dark nebula in the eastern extension of the Ophiuchus complex, and it is thus affected by a relatively high extinction [i.e., $E(B-V)=0.75$, H96; $E(B-V)=1.15$, S98]. Ortolani et al. (2003) published a [$V, V-I$] CMD showing a large field contamination and a barely detectable blue HB. From the analysis of the CMD, the authors found $E(B-V)=0.78$, $(m-M)_0=14.73$, and $[\mathrm{Fe/H}]=-1.3$ dex.

Our derived CMD, shown in Figure 2, exhibits a blue HB at $0.2 \leq (J-K) \leq 0.6$ and $14.5 \leq K \leq 16$, and a quite scattered RGB. As expected, in the [$K, J-K$]- and [$H, J-H$]-planes, the high level of contamination by disk stars strongly affecting the Ortolani et al. (2003) CMD is significantly reduced. However, in our CMD the main source of contamination is due to the foreground bulge field stars, which produce the observed RGB split. In fact, as shown in the radial CMDs of Figure 5, by increasing the distance from the cluster center a secondary red component becomes progressively more pronounced, causing the observed scatter in the RGB. As done for NGC 6256 and NGC 6293, the RGB ridgeline was derived using only the stars lying within $30''$ of the cluster center, and the main cluster properties were estimated using the empirical method of FVO06. From the observed CMDs we measured $\mathrm{RGB}_{\mathrm{slope}}=-0.068$ and $K^{\mathrm{tip}}=8.854$. Adopting these two values we found $E(B-V)=0.82$, $(m-M)_0=14.70$, $[\mathrm{Fe/H}]=-1.42$ dex, and $[\mathrm{M/H}]=-1.22$ dex for the cluster reddening, distance, and metallicity. Our findings nicely agree with the Ortolani et al. (2003) results.

3.2.7. *NGC 6388*

NGC 6388 is a moderately reddened [i.e., $E(B-V)=0.37$, H96; $E(B-V)=0.39$, S98; $E(B-V)=0.40$, Pritzl et al. 2002], metal-rich ($[\mathrm{Fe/H}]=-0.60$; H96; Pritzl et al. 2005) cluster located in the outer bulge region (see Fig. 1). Since the discovery by Rich et al. (1997) of an extended blue HB (as well as in NGC 6441) in its *HST*-based CMD, NGC 6388 has been the subject of several optical photometric studies (see, e.g., Moehler et al. 1999; Piotto et al. 2002; Pritzl et al. 2002; and references therein). NGC 6388 displays a quite peculiar HB morphology. In fact, besides a well-populated HB-RC (a feature normally predicted by stellar evolution theory in the case of old, metal-rich populations) it shows an extended blue tail and a population of

TABLE 1
Coordinates, Distance, Reddening, and Metallicity for the Global Sample of Bulge Clusters

Name (1)	l (deg) (2)	b (deg) (3)	$d_\odot$ (kpc) (4)	R_{GC} (kpc) (5)	X (kpc) (6)	Y (kpc) (7)	Z (kpc) (8)	$E(B-V)$ (9)	$(m-M)_0$ (10)	[Fe/H] (11)	[M/H] (12)	Ref. (13)
NGC 6256*	−12.21	3.31	9.1	2.2	8.9	−1.9	0.5	1.20	14.79	−1.63	−1.43	tw
NGC 6266	−6.42	7.32	6.6	1.8	6.5	−0.7	0.8	0.47	14.11	−0.99	−0.80	tw
NGC 6273*	−3.13	9.38	8.2	1.4	8.1	−0.4	1.3	0.40	14.58	−1.40	−1.21	tw
NGC 6293*	−2.38	7.83	10.5	2.8	10.4	−0.4	1.3	0.30	15.10	−1.73	−1.55	tw
NGC 6304	−4.17	5.38	6.0	2.2	5.9	−0.4	0.6	0.58	13.88	−0.75	−0.56	VOF05
NGC 6316	−2.82	5.76	11.6	3.8	11.6	−0.6	1.2	0.56	15.33	−0.58	−0.38	tw
NGC 6342	4.90	9.73	8.4	1.6	8.3	0.7	1.4	0.57	14.63	−0.71	−0.53	VFO04a
NGC 6355*	−0.42	5.43	9.0	1.1	8.7	−0.1	0.8	0.81	14.77	−1.42	−1.22	tw
NGC 6380	−9.82	−3.42	9.2	1.9	9.0	−1.6	−0.5	1.29	14.81	−0.87	−0.68	VFO04a
NGC 6388	−14.44	−6.74	11.9	4.8	11.5	−3.0	−1.4	0.44	15.38	−0.61	−0.42	tw
NGC 6401*	3.45	3.98	7.7	0.8	7.7	0.5	0.5	1.10	14.43	−1.37	−1.20	tw
NGC 6440	7.73	3.80	8.2	1.2	8.1	1.1	0.5	1.15	14.58	−0.49	−0.40	VFO04a
NGC 6441	−6.47	−5.01	13.5	5.7	13.4	−1.5	−1.2	0.52	15.65	−0.68	−0.52	VFO04a
NGC 6528	1.14	−4.17	7.5	0.8	7.5	0.1	−0.5	0.62	14.37	−0.17	+0.04	F00
NGC 6539	20.80	6.78	8.4	3.1	7.8	3.0	1.0	1.08	14.63	−0.79	−0.60	O05
NGC 6553	5.25	−3.02	4.9	3.2	4.9	0.4	−0.3	0.84	13.46	−0.30	−0.09	F00
NGC 6569	0.48	−6.68	12.0	4.2	11.9	0.1	−1.4	0.49	15.40	−0.85	−0.66	VOF05
NGC 6624	2.79	−7.91	8.4	1.3	8.3	0.4	−1.2	0.28	14.63	−0.63	−0.48	VFO04a
NGC 6637	1.70	−10.30	9.4	2.1	9.3	1.3	−1.2	0.14	14.87	−0.77	−0.57	VOF05
NGC 6638	7.90	−7.15	10.3	2.9	10.2	0.3	−1.8	0.43	15.07	−1.00	−0.78	VOF05
NGC 6642	9.81	−6.44	8.6	1.8	8.4	1.5	−1.0	0.60	14.68	−1.20	−0.99	tw
Ter 3	−14.92	9.19	8.1	2.4	7.7	−2.1	1.3	0.73	14.54	−0.82	−0.63	tw
Ter 5	3.81	1.67	5.9	2.1	5.9	0.4	0.2	2.38	13.87	−0.34	−0.14	tw
Ter 6	−1.43	−2.16	6.7	1.3	6.7	−0.2	−0.3	2.35	14.13	−0.62	−0.43	tw

Notes.—Asterisk signify clusters for which the metallicity estimates ([M/H]) were derived using the FVO06 empirical method. In the references column, "tw" signifies this work.

RR Lyrae variables (Pritzl et al. 2002). NGC 6388 and NGC 6441 are thus the most metal-rich examples of a second-parameter pair affecting the HB morphology. From the analysis of the cluster CMD based on Washington photometry, Hughes et al. (2006) claimed that NGC 6388 has a RGB too broad to be chemically homogeneous, suggesting a metallicity spread of $\delta[\mathrm{Fe/H}] \simeq 0.3$ dex. However, very recently no intrinsic metallicity spread was found by Carretta et al. (2007), who performed high-resolution ($R \approx 40{,}000$) optical spectroscopy of seven cluster members, finding an average $[\mathrm{Fe/H}] = -0.44$ dex with an rms = 0.04 dex.

No IR photometric studies have been published so far for this cluster. Figure 2 shows the first CMD in the $[K, J-K]$-plane and the derived RGB ridgeline. As expected, the observed CMD is characterized by a well-defined HB-RC, suggesting a high metallicity, while the extended blue HB is barely visible as the vertical structure at $15.5 \lesssim K \lesssim 17.5$ and $0 \lesssim (J-K) \lesssim 0.6$. The RGB appears well populated over its entire extension, from the base ($K \sim 17$) up to the tip, allowing us a detailed description of its morphological features. From the comparison of the cluster CMDs and LFs with those of 47 Tuc, we estimated the reddening and distance to be $E(B-V) = 0.44$ and $(m-M)_0 = 15.38$, respectively. The photometric indices measured along the RGB, in the $[M_K, (J-K)_0]$ and $[M_H, (J-H)_0]$ absolute planes, yielded the following metallicity estimates: $[\mathrm{Fe/H}] = -0.61$ dex and $[\mathrm{M/H}] = -0.42$ dex, in good agreement with previous literature values.

3.2.8. *NGC 6401*

NGC 6401 is located in the inner bulge region, at ∼0.8 kpc (see Table 1, Fig. 1) from the Galactic center. Its physical parameters are not well determined in the literature. In particular, the extinction estimates range from $E(B-V) = 0.53$ (Barbuy et al. 1999) to $E(B-V) = 0.98$ (S98), and the cluster distance values are between $(m-M)_0 = 14.39$ (H96) and $(m-M)_0 = 14.76$ (Barbuy et al. 1999). From the analysis of the observed $[V, V-I]$ CMD, Barbuy et al. (1999) concluded that NGC 6401 is metal-rich, with a metallicity close to that of 47 Tuc, while from low-resolution optical spectroscopy Minniti (1995) found $[\mathrm{Fe/H}] = -1.1$ dex.

The near-IR CMD obtained here is shown in Figure 2, along with the derived RGB ridgeline. The most interesting features are (1) a blue HB tail at $0.4 \leq (J-K) \leq 0.9$ and $13 \leq K \leq 16$ and (2) a rather scattered RGB, which seems split into two separate sequences, particularly in the $[K, J-K]$-plane. Note that the presence of a blue extended HB is confirmed by the Piotto et al. (2002) work based on *HST BV* observations.

Figure 6 clearly shows that in the innermost region, within 30″ of the cluster center, the CMD exhibits a blue HB and a quite narrow RGB, while for increasing distance from the cluster center, the CMD starts to be characterized by a red clumpy HB and by a RGB significantly redder than the cluster mean loci. Hence, the observed RGB spread is likely due to the bulk of the bulge field population, which is metal-rich. In order to derive the cluster main properties we used the FVO06 empirical method, assuming the bulgelike scenario. We measured the cluster RGB slope considering only those stars lying in the innermost cluster region ($\mathrm{RGB_{slope}} = -0.065$), and we estimated the observed ($K = 8.69$) RGB tip using the brightest stars in our catalog lying along the RGB ridgeline. We used these values as input parameters for the computational routine, and we obtained the following reddening, distance, and metallicity estimates: $E(B-V) = 1.1$, $(m-M)_0 = 14.43$, $[\mathrm{Fe/H}] = -1.37$ dex, and $[\mathrm{M/H}] = -1.20$ dex. The derived photometric metallicity is consistent with

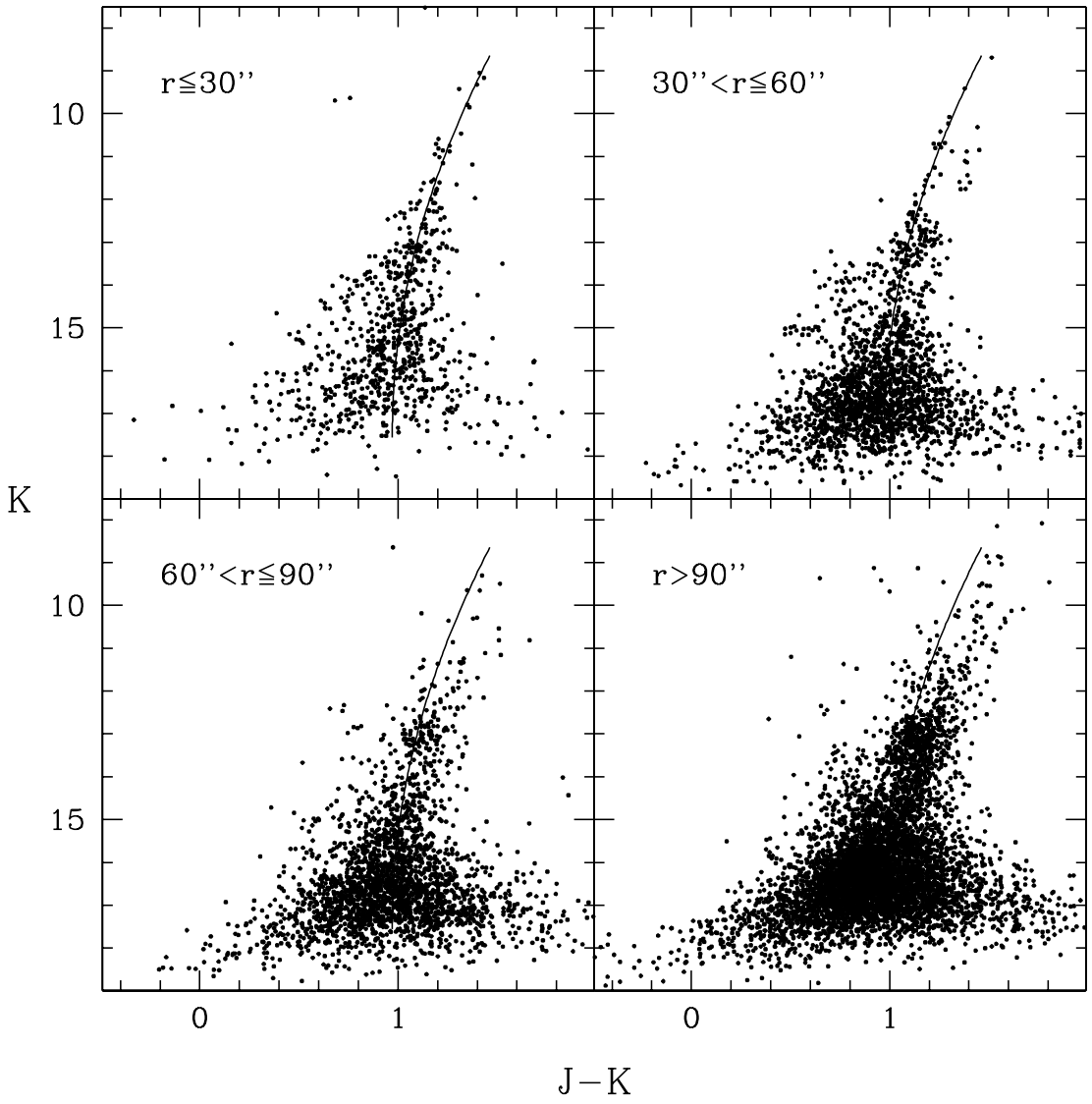

FIG. 6.—[$K, J-K$] CMDs of NGC 6401 at different distances (r) from the cluster center.

the spectroscopic result by Minniti (1995) ($\Delta[\mathrm{Fe/H}] = 0.25$ dex) and significantly lower than that found by Barbuy et al. (1999) ($\Delta[\mathrm{Fe/H}] \sim 0.7$ dex).

3.2.9. *NGC 6642*

The moderately reddened cluster NGC 6642 [i.e., $E(B-V) = 0.41$, H96; $E(B-V) = 0.40$, S98] has been observed in the IR and in the optical by Davidge (2000) and Piotto et al. (2002), respectively. However, both published CMDs show sequences that are not well populated and have a remarkable scatter. Figure 2 shows our derived CMD in the [$H, J-H$]-plane, along with the mean RGB ridgeline. The main features of the CMD are a blue HB and a steep RGB, typical of low- to intermediate-metallicity clusters. In this case, since no K photometry was available, the reddening and the distance were estimated by matching the cluster sequence loci in the CMD to those of the reference cluster NGC 6752. Using our derived reddening [$E(B-V) = 0.60$] and distance [$(m-M)_0 = 14.68$], we measured the photometric indices, giving the following photometric metallicity estimates: $[\mathrm{Fe/H}] = -1.20$ dex and $[\mathrm{M/H}] = -1.03$ dex. These values are fully consistent (within 0.2 dex) with the corresponding values listed by H96 ($[\mathrm{Fe/H}] = -1.35$) and by Minniti (1995) ($[\mathrm{Fe/H}] = -1.40$), based on low-resolution optical spectroscopy. Note that the obtained distance also nicely agrees with the value listed by H96 [i.e., $(m-M)_0 = 14.63$].

3.2.10. *Terzan 3*

Terzan 3 is a low-concentration cluster ($c = 0.70$; Djorgovski 1993) projected on the outskirts of the bulge (see Fig. 1). The only published photometry is that by Barbuy et al. (1998b). From the analysis of the derived [$V, B-V$] CMD, whose major features are a red HB and a moderately bent RGB, they derived $E(B-V) = 0.72$, $(m-M)_0 = 14.05$, and $[\mathrm{Fe/H}] \sim -0.70$ dex.

Our CMD along with the RGB fiducial ridgeline is shown in Figure 2. This high-resolution IR photometry reaches ~2 mag below the MSTO. The presence of a red clumpy HB at $K \sim 13.42$ suggests a moderately high metallicity, like that for 47 Tuc. The analysis of the cluster CMDs and LFs yields a reddening $E(B-V) = 0.73$ (in excellent agreement with the values found by Barbuy et al. [1998a] and S98), an intrinsic distance modulus $(m-M)_0 = 14.54$, and metallicities $[\mathrm{Fe/H}] = -0.82$ dex and $[\mathrm{M/H}] = -0.63$ dex. The significant (~0.5 mag) discrepancy between our distance and that of Barbuy et al. (1998b) is due to a different assumption for the selective-to-total absorption coefficient

TABLE 2

OBSERVED AND BOLOMETRIC MAGNITUDE OF THE HB RED CLUMP, RGB BUMP, AND TIP FOR THE GLOBAL SAMPLE OF BULGE CLUSTERS

Name	[Fe/H]	[M/H]	J^{RC}	H^{RC}	K^{RC}	J^{bump}	H^{bump}	K^{bump}	J^{tip}	H^{tip}	K^{tip}	M_{bol}^{bump}	M_{bol}^{tip}
NGC 6256	−1.63	−1.43	...	...	...	...	...	...	10.63	9.51	9.21	...	−3.56
NGC 6266	−0.99	−0.80	...	...	...	13.50	12.75	12.65	9.26	8.10	7.85	0.44	−3.56
NGC 6273	−1.40	−1.21	...	...	...	13.65	13.05	12.85	9.67	8.83	8.57	0.10	−3.59
NGC 6293	−1.73	−1.55	...	...	...	...	...	...	10.17	9.43	9.24	...	−3.23
NGC 6304	−0.75	−0.56	13.55	12.85	12.70	14.03	13.33	13.13	9.06	8.02	7.65	1.10	−3.59
NGC 6316	−0.58	−0.38	14.93	14.25	...	15.20	14.65	...	10.28	9.17	...	...	...
NGC 6342	−0.71	−0.53	14.25	13.60	13.40	14.65	13.85	13.75	9.71	8.67	8.35	0.98	−3.69
NGC 6355	−1.42	−1.22	...	...	...	...	...	...	10.19	9.30	8.92	...	−3.61
NGC 6380	−0.87	−0.68	14.95	14.15	13.85	15.15	14.25	13.95	10.37	9.12	8.75	0.62	−3.88
NGC 6388	−0.61	−0.42	14.90	14.27	14.17	15.18	14.47	14.33	10.24	9.47	8.81	0.88	−3.76
NGC 6401	−1.37	−1.20	...	...	...	...	...	...	10.21	9.07	8.69	...	−3.42
NGC 6440	−0.49	−0.40	14.75	13.80	13.60	15.30	14.35	14.13	10.02	8.85	8.33	1.16	−3.82
NGC 6441	−0.68	−0.52	15.20	14.55	14.40	15.70	14.85	14.77	10.47	9.49	9.12	1.10	−3.90
NGC 6528	−0.17	+0.04	14.15	...	13.35	15.10	...	14.05	9.16	...	7.85	1.74	−4.06
NGC 6539	−0.79	−0.60	14.65	13.85	13.65	14.90	14.05	13.83	10.08	8.92	8.47	0.71	−3.77
NGC 6553	−0.30	−0.09	13.35	...	12.40	14.05	...	13.05	8.56	...	6.92	1.28	−3.86
NGC 6569	−0.85	−0.66	14.95	14.40	14.25	14.93	14.23	14.08	10.52	9.49	9.21	0.55	−3.59
NGC 6624	−0.63	−0.48	13.95	13.40	13.25	14.45	13.60	13.65	9.30	8.37	8.08	1.07	−3.85
NGC 6637	−0.77	−0.57	14.05	13.65	13.55	14.28	13.78	13.65	9.91	9.08	8.72	0.69	−3.34
NGC 6638	−1.00	−0.78	14.65	14.05	13.85	14.45	13.73	13.58	9.86	8.89	8.61	0.49	−3.88
NGC 6642	−1.20	−0.99	...	...	...	13.85	13.17	...	9.92	8.92	...	...	...
Ter 3	−0.82	−0.63	14.27	13.57	13.42	14.37	13.73	13.50	9.95	8.91	8.42	0.54	−3.47
Ter 5	−0.34	−0.14	15.15	13.80	13.35	15.75	14.50	13.90	10.25	8.68	7.99	1.32	−3.96
Ter 6	−0.62	−0.43	15.10	14.07	13.48	15.75	14.45	14.00	10.56	9.06	8.33	1.01	−3.89

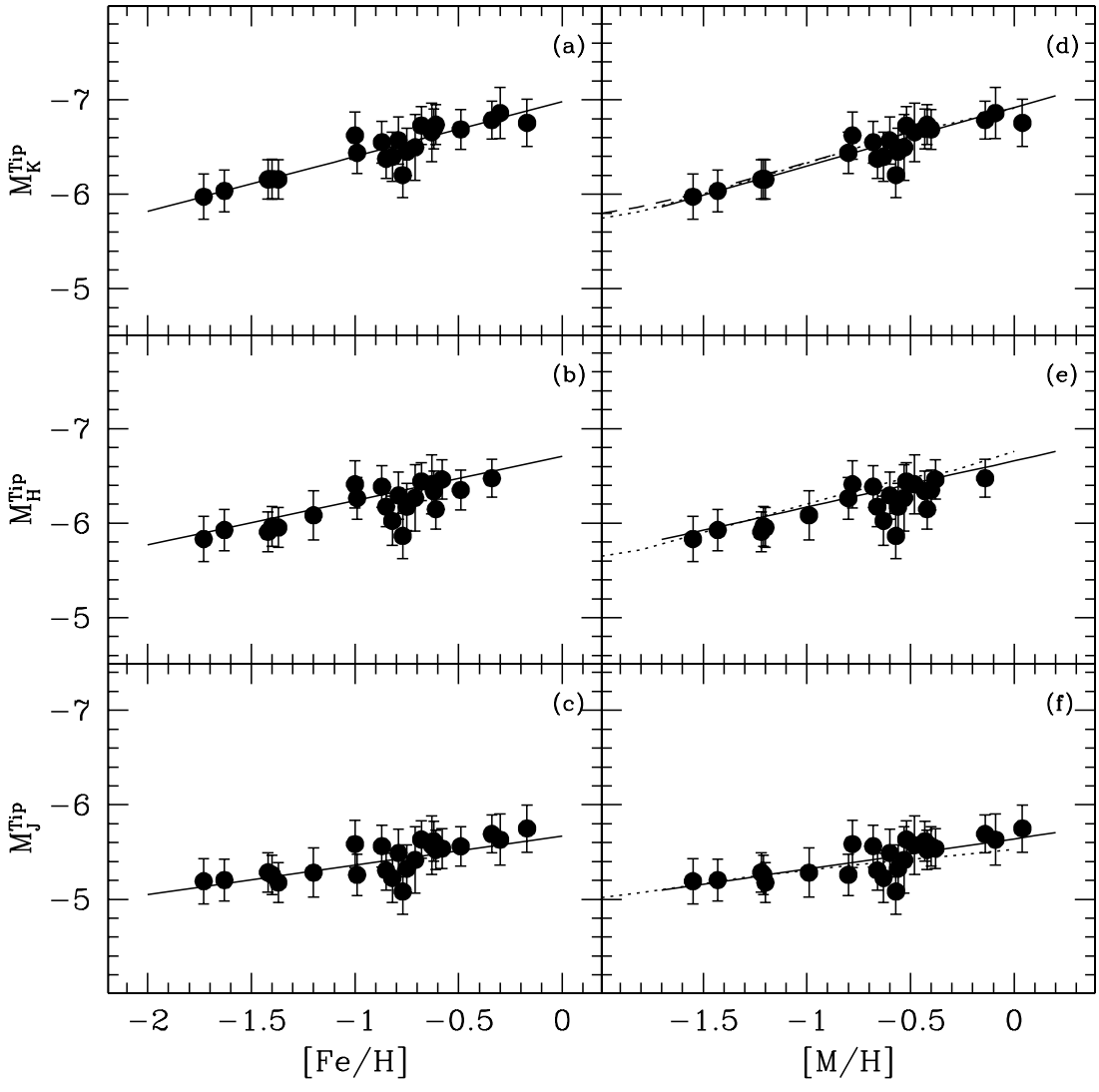

FIG. 7.—*J*, *H*, and *K* absolute magnitudes of the RGB tip as a function of the (*a*, *b*, *c*) [Fe/H] and (*d*, *e*, *f*) [M/H] metallicities for the cluster sample. The solid lines show the empirical relations from VFO04b, the dashed line shows the theoretical prediction by Straniero et al. (1997), and the dotted lines show the Cassisi et al. (2000) models.

($R_V = 3.1$ in this study; $R_V = 3.3$ in the Barbuy et al. 1998b work) and for the distance scale (that from F99 here, and that from Jones et al. [1992] in Barbuy et al. [1998b]).

3.2.11. *Terzan 5*

Terzan 5 is a compact and massive cluster located in the very inner bulge region. In the last few years this extremely dense cluster has been the subject of several studies aimed at investigating its stellar population (e.g., Ortolani et al. 1996, 2001; Cohn et al. 2002; Origlia & Rich 2004), as well as at understanding stellar interactions and GC dynamics (e.g., Heinke et al. 2003; Ransom et al. 2005), having the highest stellar interaction rate of any Galactic GC (Verbunt & Hut 1987). In fact, among GCs Ter 5 ranks first in wealth of MSPs, and it hosts many interacting binaries (e.g., cataclysmic variables and X-ray binaries). Being embedded in a heavily obscured zone, it is affected by a large differential reddening that makes optical observations almost impossible. In fact, the only available optical photometry is that by Ortolani et al. (1996), who published a CMD in the $[I, V-I]$-plane showing a largely scattered RGB and HB. They estimated $E(B-V) = 2.49$, $(m-M)_0 = 13.74$, and a metallicity close to that of NGC 6553 (i.e., $[\mathrm{Fe/H}] = -0.3$; Origlia et al. 2002). Later on, a $[J, J-H]$ CMD based on *HST* observations was published by Ortolani et al. (2001) and Cohn et al. (2002), with the aim of deriving more accurate cluster parameters such as reddening, distance, and age. From the analysis of the derived CMD, Ortolani et al. (2001) found Ter 5 to be coeval to NGC 6528. Cohn et al. (2002) obtained an IR CMD significantly deeper ($\sim$2 mag), confirming the age found by Ortolani et al. (2001). They also derived $E(B-V) = 2.16$ and $d_\odot = 8.7$ kpc.

Figure 2 shows our observed CMD in the $[K, J-K]$-plane along with the derived RGB ridgeline. The dominant features of the IR CMD are (1) a red clumpy HB and (2) a well-populated RGB, from the base ($K \sim 16$) up to the tip ($K \sim 8.5$), which allow us a clear definition of its ridgeline. From the analysis of the CMD and LF we derived $E(B-V) = 2.38$ and $(m-M)_0 = 13.87$. The reddening value is between the estimates provided by Ortolani et al. (1996) and Cohn et al. (2002), while our distance measurement is fully consistent with that of Ortolani et al. (1996). The photometric indices measured along the cluster RGB by adopting the reddening and distance quoted above lead to the metallicity estimates $[\mathrm{Fe/H}] = -0.32$ dex and $[\mathrm{M/H}] = -0.19$ dex, thus in excellent agreement with the high-resolution IR spectroscopic result obtained by Origlia & Rich (2004) ($[\mathrm{Fe/H}] = -0.21$ dex).

3.2.12. *Terzan 6*

Terzan 6 is another example of a heavily reddened cluster in the inner bulge region. The only available photometric study is the one by Barbuy et al. (1997), which provided a $[I, V-I]$ CMD. The authors estimated the cluster reddening [$E(B-V) = 2.24$] by comparing the derived CMD with that of NGC 6553, and the cluster distance [$(m-M)_0 = 14.23$] using the absolute V magnitude of the HB level, and from the RGB morphology they concluded that Ter 6 shows intermediate characteristics between those of 47 Tuc and NGC 6528/NGC 6553.

Our IR observations of Ter 6 provided the first IR CMD (see Fig. 2), showing a red HB and a curved RGB, which are both high-metallicity indicators. From the derived CMD we found $E(B-V) = 2.35$ and $(m-M)_0 = 14.13$. Both estimates nicely agree with the corresponding values found by Barbuy et al. (1997). The set of IR photometric indices measured using the RGB ridgelines gives a cluster metallicity of $[\mathrm{Fe/H}] = -0.62$ dex and $[\mathrm{M/H}] = -0.43$ dex.

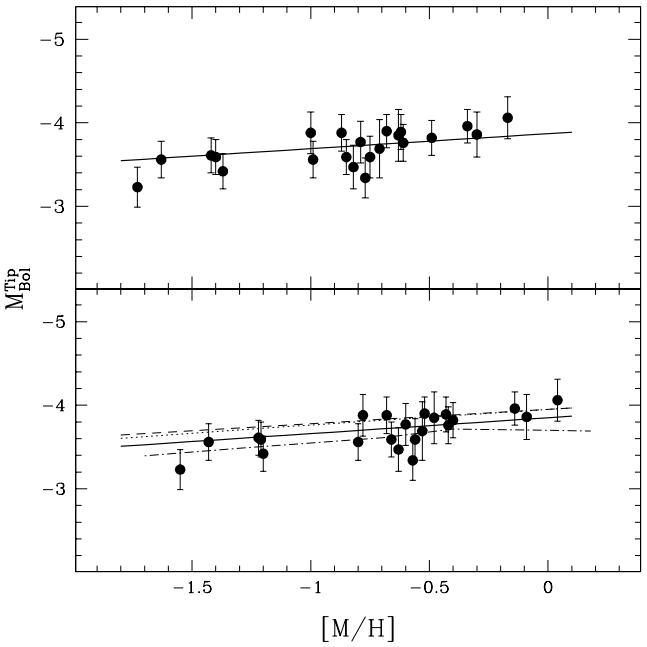

FIG. 8.—Bolometric magnitudes of the RGB tip as a function of the cluster [Fe/H] (*top*) and [M/H] (*bottom*) metallicities. The solid lines show the empirical relation from VFO04b. Three theoretical predictions have been plotted in the bottom panel: Caloi et al. (1997; *dashed line*), Salaris & Cassisi (1997; *dotted line*), and Girardi et al. (2000; *dot-dashed line*).

4. THE FINAL COMPILATION

The compilation presented in this study is publicly available either by anonymous FTP or through the World Wide Web.[4] For the entire cluster sample, two separate files are available: the first lists the J, H, and K photometry for all the measured stars in each cluster, together with the stars' absolute positions in right ascension and declination; the second reports the observed RGB fiducial ridgeline in the $[K, J-K]$- and $[H, J-H]$-planes.

Table 1 lists the derived parameters for the 24 clusters, namely, the reddening, the distance, and the metallicity in both adopted scales (cols. [9], [10], [11], and [12], respectively). Moreover, using our distance determinations and the (l, b) Galactic coordinates from H96, and assuming a distance $R_0 = 8$ kpc to the Galactic center (Eisenhauer et al. 2003), we also provide new estimates of the clusters' distances from the Sun ($d_\odot$) and from the Galactic center (R_{GC}), and the distance components X, Y, Z in a Sun-centered coordinate system (cols. [4], [5], [6], [7], and [8], respectively). Finally, for each cluster column (13) lists the references for the IR photometry. It is worth mentioning that Table 1 lists the largest homogeneous compilation of bulge GCs obtained so far, whose properties were derived in a self-consistent way. In fact, the derived cluster reddenings, distances, and metallicities are based on (1) a homogeneous photometric database analyzed using the same data reduction procedures, and calibrated onto the 2MASS photometric system; (2) the F99 distance scale; and (3) a uniform and high-resolution metallicity scale (Carretta & Gratton 1997). A summary table with the derived parameters for the global sample of clusters, here split into Tables 1 and 2, is also provided in an easily machine-readable format on our Web site.

4.1. *The RGB Bump and Tip*

The most interesting evolutionary features along the RGB are the so-called bump and tip. The former flags the point (during

[4] The Web site address is http://www.bo.astro.it/~GC/ir_archive.

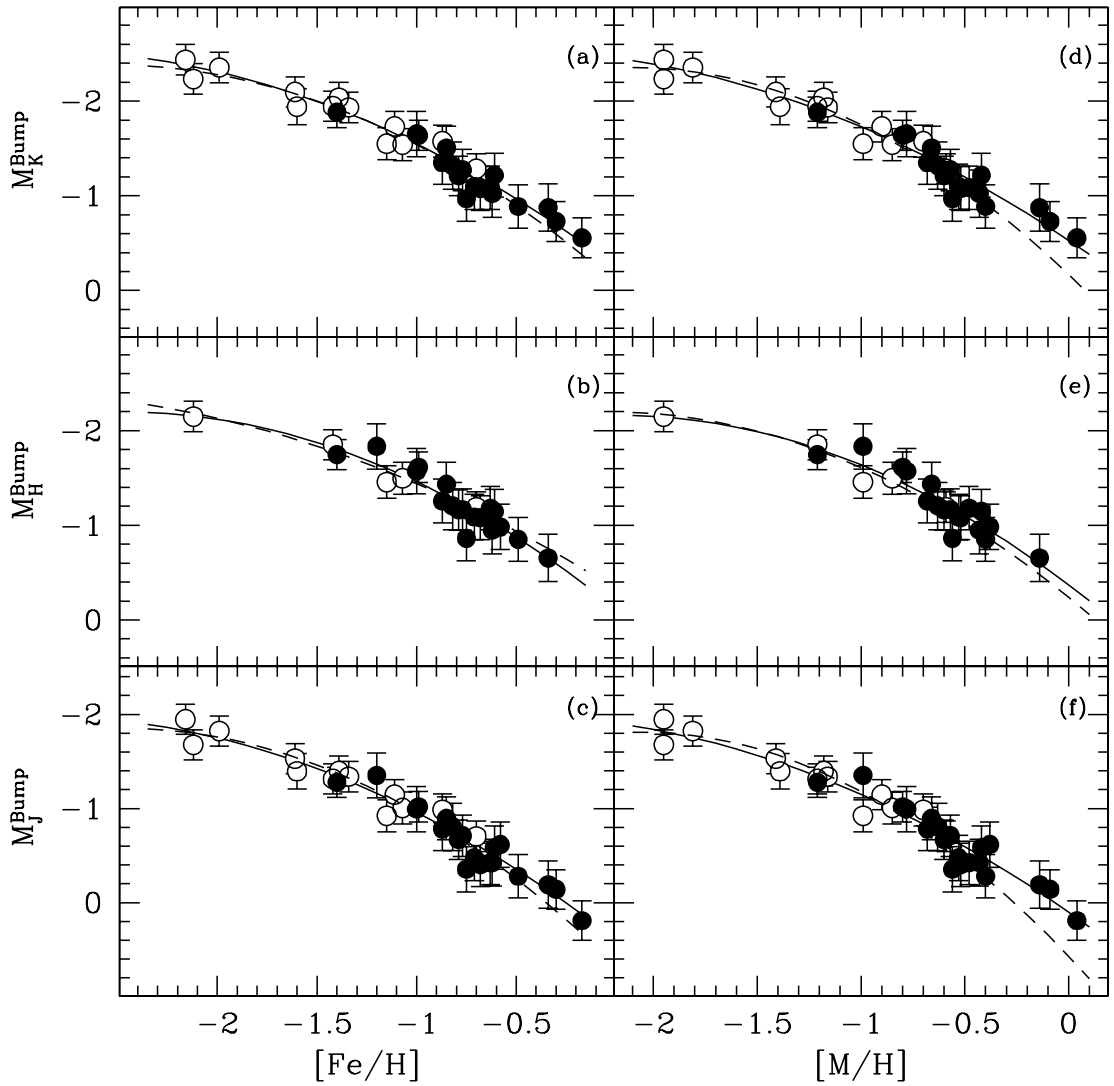

FIG. 9.—*J*, *H*, and *K* absolute magnitudes of the RGB bump as a function of the cluster (*a*, *b*, *c*) [Fe/H] and (*d*, *e*, *f*) [M/H] metallicities. Filled circles indicate program bulge clusters, and open circles indicate halo clusters presented in VFO04b. The solid lines show the new best-fitting relations. The dashed lines show the VFO04b calibrations.

the post-MS evolution of low-mass stars) when the narrow hydrogen-burning shell reaches the discontinuity in the hydrogen distribution profile, generated by the previous innermost penetration of the convective envelope. Besides providing an obvious check on the accuracy of theoretical models of stellar evolution, the identification of the RGB bump in stellar systems can be a useful tool for providing observational constraints on a number of population parameters, since it is a sensitive function of metal content, helium abundance, and stellar population age. From the observational point of view, as emphasized by Fusi Pecci et al. (1990) and F99, the combined use of the differential and integrated LFs is the best tool to properly detect the bump.

The evolution along the RGB ends at the so-called RGB tip with helium ignition in the stellar core. In GC stars this event is moderately violent because it takes place in an electron-degenerate core. Because the RGB reaches its maximum extension in luminosity for stellar populations older than $\tau \approx 1$–2 Gyr (i.e., when stars with $M \leq 2.0\,M_{\odot}$ are evolving off the MS) and it remains approximately constant with increasing age of the population, the tip is now widely used as a standard candle for distance determination of stellar systems.

The dependence of the RGB bump and tip luminosities (in the *J*, *H*, and *K* bands, as well as bolometric) on the cluster metallicity has been investigated in VFO04b. Here we have extended the same study to the new sample of bulge clusters. In doing this, we have adopted the same strategy followed in that paper, in which the reader can find a detailed description of the adopted procedures.

For the entire sample, the measurements of the main evolutionary features are listed in Table 2: the observed *J*, *H*, and *K* magnitude of the HB-RC (cols. [4], [5], and [6]), and the *J*, *H*, *K*, and bolometric bump (cols. [7], [8], [9], and [13], respectively) and tip (cols. [10], [11], [12], and [14], respectively) magnitudes. The bolometric bump and tip magnitude were obtained using the bolometric corrections for Population II giants computed by Montegriffo et al. (1998).

Figure 7 shows the absolute RGB tip magnitudes as a function of the metallicity, in both adopted scales. The clusters' tip determinations nicely agree with the empirical relations by VFO04b (*solid lines*) and with the theoretical predictions by Straniero et al. (1997) and Cassisi et al. (2000) (*dashed and dotted lines, respectively*). As shown in Figure 8, a good agreement is also

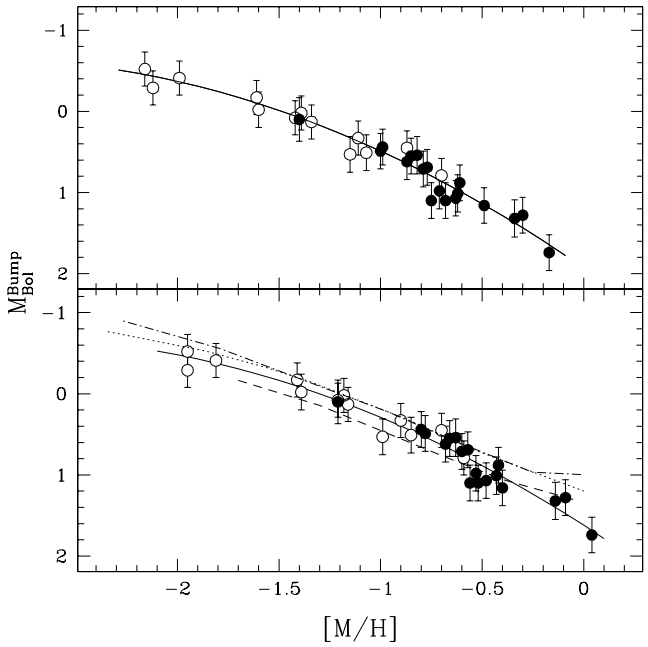

FIG. 10.—Bolometric magnitudes of the RGB bump as a function of the cluster [Fe/H] (*top*) and [M/H] (*bottom*) metallicities. Filled circles indicate program bulge clusters, and open circles indicate halo clusters presented in VFO04b. The solid lines show our best-fitting relations. Three theoretical predictions have been plotted in the bottom panel: Straniero et al. (1997; *dotted line*), Girardi et al. (2000; *dashed line*), and Pietrinferni et al. (2004; *dash-dotted line*).

found when we compare the bolometric tip magnitudes, as a function of cluster metallicity, with the VFO04b empirical relation (*solid lines*) and with three different theoretical expectations by Caloi et al. (1997), Salaris & Cassisi (1997), and Girardi et al. (2000) (*dashed, dotted, and dot-dashed lines, respectively*).

Figure 9 plots the absolute J, H, and K bump magnitudes of the bulge (*filled circles*) and halo (*open circles*) clusters (the latter presented in VFO04b) versus metallicity, showing that the bump becomes rapidly fainter by increasing the latter. Hence, since with the present study we both enlarged the sample of high-metallicity clusters and adopted the recent [Fe/H] estimates by Origlia et al. (2002, 2005a) based on high-resolution IR spectroscopy, for the two most metal-rich objects in our sample (namely, NGC 6528 and NGC 6553), we calibrated new relations. As shown in Figure 9 the new calibrations (*solid lines*) differ from the VFO04b ones (*dashed lines*) only in the metal-rich tail, making the bump somewhat brighter. The new calibrations of the bump J, H, and K absolute magnitudes, in both adopted metallicity scales, are as follows:

$$M_J^{\rm bump} = 0.39 + 1.63[{\rm Fe/H}] + 0.28[{\rm Fe/H}]^2, \quad (1)$$

$$M_H^{\rm bump} = -0.12 + 1.68[{\rm Fe/H}] + 0.34[{\rm Fe/H}]^2, \quad (2)$$

$$M_K^{\rm bump} = -0.25 + 1.57[{\rm Fe/H}] + 0.27[{\rm Fe/H}]^2, \quad (3)$$

$$M_J^{\rm bump} = 0.10 + 1.53[{\rm M/H}] + 0.28[{\rm M/H}]^2, \quad (4)$$

$$M_H^{\rm bump} = -0.37 + 1.65[{\rm M/H}] + 0.38[{\rm M/H}]^2, \quad (5)$$

$$M_K^{\rm bump} = -0.53 + 1.47[{\rm M/H}] + 0.27[{\rm M/H}]^2. \quad (6)$$

Figure 10 shows the bolometric magnitude of the bump as a function of the cluster metallicity, together with the new best-fit relations:

$$M_{\rm Bol}^{\rm bump} = 1.93 + 1.73[{\rm Fe/H}] + 0.29[{\rm Fe/H}]^2, \quad (7)$$

$$M_{\rm Bol}^{\rm bump} = 1.62 + 1.61[{\rm M/H}] + 0.28[{\rm M/H}]^2. \quad (8)$$

The comparison between the data and the theoretical models by Straniero et al. (1997), Girardi et al. (2000), and Pietrinferni et al. (2004) (see Fig. 10, *bottom*) shows an overall good agreement.

Part of the data analysis was performed with software developed by P. Montegriffo at the Osservatorio Astronomico di Bologna (INAF). The Ministero dell'Istruzione, dell'Universitá e della Ricerca is kindly acknowledged for financial support. We warmly thank the ESO La Silla Observatory staff for assistance during the observations. This publication makes use of data products from the Two Micron All Sky Survey, which is a joint project of the University of Massachusetts and Infrared Processing and Analysis Center/California Institute of Technology, funded by the National Aeronautics and Space Administration and the National Science Foundation.

REFERENCES

Barbuy, B., Bica, E., & Ortolani, S. 1998a, A&A, 333, 117
Barbuy, B., Ortolani, S., & Bica, E. 1997, A&AS, 122, 483
———. 1998b, A&AS, 132, 333
Barbuy, B., Ortolani, S., Bica, E., & Desidera, S. 1999, A&A, 348, 783
Beccari, G., Ferraro, F. R., Possenti, A., Valenti, E., Origlia, L., & Rood, R. T. 2006, AJ, 131, 2551
Bica, E., Clariaa, J. J., Piatti, A. E., & Bonatto, C. 1998, A&AS, 131, 483
Caloi, V., D'Antona, F., & Mazzitelli, I. 1997, A&A, 320, 823
Carney, B. W. 1996, PASP, 108, 900
Carretta, E., & Gratton, R. G. 1997, A&AS, 121, 95
Carretta, E., et al. 2007, A&A, in press (astro-ph/0701176)
Cassisi, S., Castellani, V., Ciarcelluti, P., Piotto, G., & Zoccali, M. 2000, MNRAS, 315, 679
Cohn, H. N., Lugger, P. H., Grindlay, J. E., & Edmonds, P. D. 2002, ApJ, 571, 818
Contreras, R., Catelan, M., Smith, H. A., Pritzl, B. J., & Borissova, J. 2005, ApJ, 623, L117
Cunha, K., & Smith, V. V. 2006, ApJ, 651, 491
Davidge, T. J. 2000, AJ, 120, 1853
Davidge, T. J., Harris, W. E., Bridges, T. J., & Hanes, D. A. 1992, ApJS, 81, 251
Dinescu, D. I., Girard, T. M., van Altena, W. F., & Lopez, C. E. 2003, AJ, 125, 1373
Djorgovski, S. 1993, in ASP Conf. Ser. 50, Structure and Dynamics of Globular Clusters, ed. S. Djorgovski & G. Meylan (San Francisco: ASP), 373
Eisenhauer, F., Schodel, R., Genzel, R., Ott, T., Tecza, M., Abuter, R., Eckart, A., & Alexander, T. 2003, ApJ, 597, L121
Ferraro, F. R., Messineo, M., Fusi Pecci, F., De Paolo, M. A., Straniero, O., Chieffi, A., & Limongi, M. 1999, AJ, 118, 1738 (F99)
Ferraro, F. R., Montegriffo, P., Origlia, L., & Fusi Pecci, F. 2000, AJ, 119, 1282 (F00)
Ferraro, F. R., Valenti, E., & Origlia, L. 2006, ApJ, 649, 243 (FVO06)
Fulbright, J. P., McWilliam, A., & Rich, M. R. 2006, ApJ, submitted (astro-ph/0609087)
Fusi Pecci, F., Ferraro, F. R., Crocker, D. A., Rodd, T. R., & Buonanno, R. 1990, A&A, 238, 95
Girardi, L., Bressan, A., Bertelli, G., & Chiosi, C. 2000, A&AS, 141, 371
Harris, W. E. 1996, AJ, 112, 1487 (H96) (for the 2003 updated version see http://physwww.mcmaster.ca/~harris/mwgc.dat)
Heinke, C. O., Edmonds, P. D., Grindlay, J. E., Lloyd, D. A., Cohn, H. N., & Lugger, P. M. 2003, ApJ, 590, 809
Hughes, J. D., Wallerstein, G., Covarrubias, R., & Hays, N. 2006, BAAS, 208, 6501
Jones, R. V., Carney, B. W., Storm, J., & Latham, D. W. 1992, ApJ, 386, 646
Lee, J.-W., & Carney, B. W. 2002, AJ, 124, 1511
Minniti, D. 1995, A&A, 303, 468
Moehler, S., Sweigart, A. V., & Catelan, M. 1999, A&A, 351, 519

Montegriffo, P., Ferraro, F. R., Origlia, O., & Fusi Pecci, F. 1998, MNRAS, 297, 872
Origlia, L., & Rich, R. M. 2004, AJ, 127, 3422
Origlia, L., Rich, R. M., & Castro, S. 2002, AJ, 123, 1559
Origlia, L., Valenti, E., & Rich, R. M. 2005a, MNRAS, 356, 1276
Origlia, L., Valenti, E., Rich, R. M., & Ferraro, F. R. 2005b, MNRAS, 363, 897 (O05)
Ortolani, S., Barbuy, B., & Bica, E. 1996, A&A, 308, 733
Ortolani, S., Barbuy, B., Bica, E., Renzini, A., Zoccali, M., Rich, R. M., & Cassisi, S. 2001, A&A, 376, 878
Ortolani, S., Bica, E., & Barbuy, B. 2003, A&A, 402, 565
Pietrinferni, A., Cassisi, S., Salaris, M., & Castelli, F. 2004, ApJ, 612, 168
Piotto, G., Zoccali, M., King, I. R., Djorgovski, S. G., Sosin, D., Rich, R. M., & Meylan, G. 1999, AJ, 118, 1727
Piotto, G., et al. 2002, A&A, 391, 945
Possenti, A., D'Amico, N., Manchester, R. N., Camilo, F., Lyne, A. G., Sarkissian, J., & Corongiu, A. 2003, ApJ, 599, 475
Pritzl, B. J., Smith, H. A., Catelan, M., & Sweigart, A. V. 2002, AJ, 124, 949
Pritzl, B. J., Venn, K. A., Ivans, I. I., Catelan, M., Layden, A. C., Kinemuchi, K., Rich, R. M., & Sweigart, A. V. 2005, BAAS, 206, 3601
Ransom, S. M., Hessels, J. W., Stairs, I. H., Freire, P. C. C., Camilo, F., Kaspi, V. M., & Kaplan, D. L. 2005, Science, 307, 892
Rich, R. M., & Origlia, L. 2005, ApJ, 634, 1293
Rich, R. M., et al. 1997, ApJ, 484, L25
Salaris, M., & Cassisi, S. 1997, MNRAS, 289, 406
Schlegel, D. J., Finkbeiner, D. P., & Davis, M. 1998, ApJ, 500, 525 (S98)
Stephens, A. W., & Frogel, J. A. 2004, AJ, 127, 925
Stetson, P. B. 1987, PASP, 99, 191
Straniero, O., Chieffi, A., & Limongi, M. 1997, ApJ, 490, 425
Valenti, E., Ferraro, F. R., & Origlia, L. 2004a, MNRAS, 351, 1204 (VFO04a)
———. 2004b, MNRAS, 354, 815 (VFO04b)
Valenti, E., Ferraro, F. R., Perina, S., & Origlia, L. 2004c, A&A, 419, 139
Valenti, E., Origlia, L., & Ferraro, F. R. 2005, MNRAS, 361, 272 (VOF05)
Verbunt, F., & Hut, P. 1987, in IAU Symp. 125, The Origin and Evolution of Neutron Stars, ed. D. J. Helfand & H. H. Huang (Dordrecht: Reidel), 187
Weiland, J. L., et al. 1994, ApJ, 425, L81
Zoccali, M., et al. 2004, A&A, 423, 507
———. 2006, A&A, 457, L1